Colloids and Surfaces B: Biointerfaces 219 (2022) 112828

Contents lists available at ScienceDirect

Colloids and Surfaces B: Biointerfaces

journal homepage: www.elsevier.com/locate/colsurfb

Organoselenium compounds as functionalizing agents for gold nanoparticles in cancer therapy

Sara Lorenzoni [a], Sara Cerra [a,*], Eduardo Angulo-Elizari [b], Tommaso A. Salamone [a], Chiara Battocchio [c], Martina Marsotto [c], Francesca A. Scaramuzzo [d], Carmen Sanmartín [b], Daniel Plano [b,*], Ilaria Fratoddi [a]

[a] Department of Chemistry, Sapienza University of Rome, P.le A. Moro 5, 00185 Rome, Italy
[b] Department of Pharmaceutical Technology and Chemistry, University of Navarra, Irunlarrea 1, Pamplona E-31008, Spain
[c] Department of Sciences, Roma Tre University, Via della Vasca Navale 79, 00146 Rome, Italy
[d] Department of Basic and Applied Sciences for Engineering (SBAI), Sapienza University of Rome, Via Antonio Scarpa 14, 00161 Rome, Italy

ARTICLE INFO

Keywords:
Hydrophilic gold nanoparticles
Organoselenium compounds
Se-functionalized AuNPs
HCT-116 cell line
PC-3 cell line
Drug delivery

ABSTRACT

Gold nanoparticles (AuNPs) modified with four organoselenium compounds, *i.e.*, 4-selenocyanatoaniline (compound **1**), 4,4′-diselanediyldianiline (compound **2**), *N*-(4-selenocyanatophenyl)cinnamamide (compound **3**), and *N*-(3-selenocyanatopropyl)cinnamamide (compound **4**), were synthesized following two different approaches: direct conjugation and non-covalent immobilization onto hydrophilic and non-cytotoxic AuNPs functionalized with 3-mercapto-1-propanesulfonate (3MPS). Both free compounds and AuNPs-based systems were characterized *via* UV-Vis, FTIR NMR, mass spectrometry, and SR-XPS to assess their optical and structural properties. Size and colloidal stability were evaluated by DLS and ζ-potential measurements, whereas morphology at solid-state was evaluated by atomic force (AFM) and scanning electron (FESEM) microscopies. AuNPs synthesized through chemical reduction method in presence of Se-based compounds as functionalizing agents allowed the formation of aggregated NPs with little to no solubility in aqueous media. To improve their hydrophilicity and stability mixed AuNPs-3MPS-**1** were synthesized. Besides, Se-loaded AuNPs-3MPS revealed to be the most suitable systems for biological studies in terms of size and colloidal stability. Selenium derivatives and AuNPs were tested *in vitro via* MTT assay against PC-3 (prostatic adenocarcinoma) and HCT-116 (colorectal carcinoma) cell lines. Compared to free compounds, direct functionalization onto AuNPs with formation of Au-Se covalent bond led to non-cytotoxic systems in the concentration range explored (0–100 μg/mL), whereas immobilization on AuNPs-3MPS improved the cytotoxicity of compounds **1**, **3,** and **4**. Selective anticancer response against HCT-116 cells was obtained by AuNPs-3MPS-**1**. These results demonstrated that AuNPs can be used as a platform to tune the *in vitro* biological activity of organoselenium compounds.

1. Introduction

Nanostructured materials are used in optical, electronic, biomedical, and environmental fields among other areas. Noble metal nanoparticles (MNPs) find application in drug delivery for complex disease therapies [1,2]. MNPs possess peculiar size-dependent properties, *i.e.*, scattering and absorption of light in the UV–vis range, as the localized surface plasmon resonance (LSPR) phenomenon that makes them useful for molecular biosensors and *in vivo* diagnostics [3,4]. In biomedical applications, NPs-based drug delivery systems display reduced systemic toxicity compared to free drug formulations [5–7]. Viability of these colloidal systems depends on purity, size, surface charge, and functionalizing layer, among other factors [8–10]. In literature, there are many synthetic protocols for MNPs synthesis, the most common being bottom-up methods in the presence of capping agents [11,12]. Alternatively, plant-mediated green synthesis approach can be used to synthesize nanoparticles, especially gold nanoparticles, with non-hazard and biocompatible features along with biological activities [10,13]. The most widely used functionalizing agents for the stabilization of the colloidal dispersion are alkane/aryl thiols [14,15]. Despite major drawbacks in the use of thiol functionalizing ligands and inorganic reducing agents compared to biological sources (plants, bacteria, or

* Corresponding authors.
E-mail addresses: sara.cerra@uniroma1.it (S. Cerra), dplano@unav.es (D. Plano).

https://doi.org/10.1016/j.colsurfb.2022.112828
Received 10 June 2022; Received in revised form 24 July 2022; Accepted 1 September 2022
Available online 7 September 2022

fungi), a fine tune of the surface properties, size distribution, and stability of AuNPs can be obtained. Due to similar chemical properties of selenium (Se) and sulfur (S), selenate anions could offer an alternative to thiolates as capping agents for MNPs. Se-based ligands can show advantages over thiols in cancer therapy such as reduced interference effect with thiolate molecules in biological environment, *e.g.*, glutathione (GSH), high efficacy and selectivity against cancer cells, along with pro-oxidant effects [16,17]. Being essential in different physiological functions, selenium plays an important role in human health [18]. Se supplementation, depending on its chemical form, dose, and metabolism, revealed to be helpful as therapeutic agent [19,20]. In cancer, many Se-based compounds have been described as chemopreventive and cytotoxic agents based on a multi-targeting effect triggering different pathways of death signaling and inhibiting tumor formation and metastasis [20–23]. Among others, selenocyanates and diselenides are known to exhibit potent antitumoral activity [24,25]. Nanosized Se showed to upregulate selenoenzyme activity with low level of toxicity [26–28]. Herein, the synthesis, characterization, and *in vitro* cytotoxic activity of Se compounds and organoselenium-functionalized AuNPs are reported. The Se-containing ligands used as capping agents for AuNPs were synthesized starting from 4-selenocyanatoaniline as a building block [29]. Two strategies for the synthesis of AuNPs were followed: (i) direct conjugation *via* single phase chemical reduction method starting from $HAuCl_4$ as gold precursor in presence of Se ligands, *i.e.*, 4-selenocyanatoaniline (4SCA, compound **1**), 4,4′-diselanediyldianiline (4DDA, compound **2**), *N*-(4-selenocyanatophenyl)cinnamamide (4NSC, compound **3**), and *N*-(3-selenocyanatopropyl)cinnamamide (3SCPC, compound **4**), as functionalizing agents [12]; (ii) non-covalent immobilization approach of the Se compounds onto hydrophilic AuNPs stabilized by 3-mercapto-1-propanesulfonate (AuNPs-3MPS) [1]. Pristine organoselenium compounds and Se-functionalized AuNPs were tested *in vitro* on HCT-116 (human colon carcinoma), and PC-3 (prostate cancer) cell lines to evaluate their toxicity and half maximal inhibitory concentration (IC_{50}).

2. Experimental section

2.1. Materials and methods

All reagents were purchased from Sigma-Aldrich and PanReac AppliChem at the highest available purity and used as received. A complete list of the reagents, solvents, and characterization techniques can be found in Supporting Information.

Dynamic light scattering (DLS) measurements were carried out with a Malvern Zetasizer Nano-ZS90 instrument. Results were reported as average hydrodynamic diameter ($<2R_H>$ nm) ± standard deviation over three measurements. Colloidal stability in H_2O_{up} was evaluated by ζ-potential measurements. Morphological characterizations of the AuNPs were carried out with field-emission scanning electron (FESEM) AURIGA Zeiss and Atomic Force (AFM) Multimode™ microscopes.

SR-XPS (Synchrotron Radiation Induced X-ray Photoelectron Spectroscopy) experiments were carried out at the SuperESCA beamline at the ELETTRA synchrotron facility of Trieste (Italy). Further details on data acquisition and analysis are reported in Supporting Information.

2.1.1. Synthesis of 4-selenocyanatoaniline

The synthesis of 4-selenocyanatoaniline (4SCA, compound **1**) was performed according to previous work [29]. Compound **1** was synthesized by adding selenium dioxide (3.09 g, 27.03 mmol) to a stirring solution of malononitrile (0.92 g, 13.93 mmol) in a 2:1 molar ratio in DMSO (15 mL). The mixture was allowed to react at room temperature for 1 h to obtain triselenium dicyanide. Then, aniline (1.90 mL, 20.89 mmol) was added, and the mixture stirred for 2 h; then added on ice cold water (150 mL). The resulting precipitate was filtered off, dissolved in diethyl ether, dried, and recrystallized from a mixture of methanol:H_2O (1:1 v/v).

2.1.2. Synthesis of 4,4′-diselanediyldianiline

4,4′-diselanediyldianiline (4DDA, compound **2**), was obtained by reduction of 4-selenocyanatoaniline (compound **1**) with sodium borohydride in a compound **1**:$NaBH_4$ 4:1 molar ratio [29]. $NaBH_4$ (0.10 g, 2.50 mmol) was added to compound **1** (2.00 g, 10.15 mmol) in absolute ethanol (40 mL) under constant stirring. The mixture was stirred for 30 min at room temperature, then the product was precipitated in water, filtered off, washed with n-hexane, and air dried.

2.1.3. Synthesis of N-(4-selenocyanatophenyl)cinnamamide

N-(4-selenocyanatophenyl)cinnamamide (4NSC, compound **3**) was obtained by reaction of 4-selenocyanatoaniline (compound **1**, 2.66 g, 13.50 mmol) with cinnamoyl chloride (compound **0**, 2.25 g, 13.50 mmol) in DCM (50 mL), and in the presence of triethylamine (TEA, 1.87 mL, 13.50 mmol). The resulting mixture was stirred at room temperature for 24 h. Then, the mixture was heated under reflux for 6 h. The precipitate was filtered off and air dried.

2.1.4. Synthesis of N-(3-selenocyanatopropyl)cinnamamide

For the synthesis of *N*-(3-selenocyanatopropyl)cinnamamide (3SCPC, compound **4**), 3-bromopropylamine hydrobromide (compound **0a**, 2.62 g, 12 mmol) was added to cinnamoyl chloride (compound **0**, 2.00 g, 12 mmol) and triethylamine (3.28 mL, 12 mmol) in DCM (50 mL), under constant stirring to obtain compound **0b**. The mixture was stirred under reflux for 10 h. The product compound **0b** was isolated by organic extraction in a separatory funnel (3 × DCM/H_2O) and dried with anhydrous Na_2SO_4. The reaction yield obtained from the first step after purification by chromatographic column using hexane/ethyl acetate as eluents was 43 % (1.30 g, 5.20 mmol). Potassium selenocyanate (0.74 g, 5.20 mmol) was added to a stirring acetonitrile solution (50 mL) of compound **0b** from the first step under reflux conditions and stirred for 30 h. The KBr precipitate was filtered off, the solvent was eliminated by rotatory evaporation; then, the residue was extracted with 3 × DCM/H_2O and purified by chromatographic column using hexane/ethyl acetate as eluents.

2.1.5. Synthesis of functionalized gold nanoparticles

Functionalized gold nanoparticles, *i.e.*, AuNPs-4SCA, AuNPs-4NSC, AuNPs-3SCPC, and AuNPs-3MPS-4DDA hereafter reported as AuNPs-**1**, AuNPs-**3** and AuNPs-**4**, and AuNPs-3MPS-**1**, respectively, were prepared *via* a single phase chemical reduction method starting from $HAuCl_4$ in the presence of the Se ligands and $NaBH_4$ as the reducing agent in the following molar ratios: Au/**1**/$NaBH_4$ 1/4/50, Au/**3**/$NaBH_4$ 1/2/20, Au/**4**/$NaBH_4$ 1/4/20, and mixed Au/3MPS/**2**/$NaBH_4$ 1/4/2/20. Briefly, gold (III) chloride trihydrate (50 mg, 1.27 mmol) was dissolved in 5 mL of THF in a two-neck round bottom flask. Subsequently, THF solution of the corresponding organoselenium compound was added and the mixture degassed under Ar flux for 10 min. Then, an aqueous solution of $NaBH_4$ was added dropwise to the reaction mixture. The reaction was carried out under vigorous stirring at room temperature for 2 h. All products were purified by repeated washing steps in centrifuge (THF, 13400 rpm, +8 °C, 20 min). For the preparation of AuNPs with mixed ligands, *i.e.*, AuNPs-3MPS-**1**, 3MPS was dissolved in 5 mL of H_2O_{up} and added to the reaction mixture after the organoselenium compound.

2.1.6. Loading of organoselenium compounds on AuNPs-3MPS

AuNPs-3MPS@4SCA, AuNPs-3MPS@4NSC, and AuNPs-3MPS@3SCPC hereafter reported as AuNPs-3MPS@**1**, AuNPs-3MPS@**3** and AuNPs-3MPS@**4**, respectively, were prepared by non-covalent conjugation method of Se-containing compounds on hydrophilic AuNPs-3MPS (2 mg/mL), synthesized as described in the literature [1]. The immobilization procedure was performed in H_2O_{up} (pH 7) at R.T. for 4 h under mild stirring in a AuNPs-3MPS@Se-based compound 10:1 wt/wt. The loading percentage was evaluated by interpolation of the UV-Vis calibration curve in H_2O_{up} at λ_{max} of each Se compound: $\lambda_{\mathbf{1}}$ = 260 nm ($\varepsilon_{260} = 4973\ M^{-1}\ cm^{-1}$), $\lambda_{\mathbf{3}} = 305$ nm ($\varepsilon_{305} = 46343\ M^{-1}\ cm^{-1}$),

$\lambda_4 = 275$ nm ($\varepsilon_{275} = 24499\ M^{-1}\ cm^{-1}$). The drug loading percentage was calculated using the following equation:

$$\%Loading = \frac{(mol\ drug_{initial} - mol\ drug_{superntant})}{mol\ drug_{initial}} \times 100$$

Loading compound **1** = (47 ± 4 %, 238 ± 22 μM), loading compound **3** = (64 ± 2 %, 195 ± 5 μM), loading compound **4** = (46 ± 5 %, 157 ± 18 μM). Stability studies of AuNPs (1 mg/mL) were carried out in H_2O_{up} (pH 7) at 37 °C. Release studies were done at 30, 60, 120, 180 min and 24 h, on the supernatant using the standard curve.

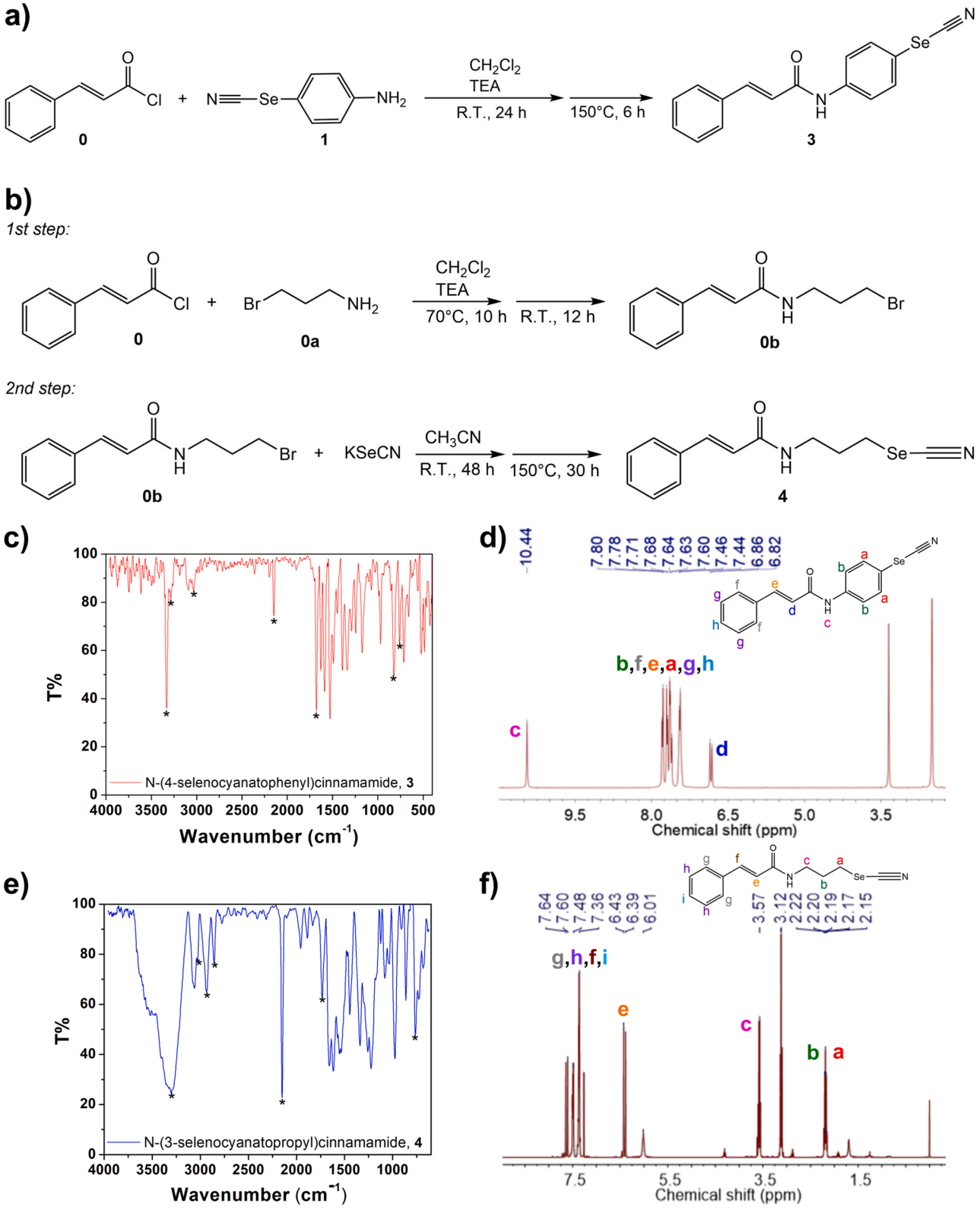

Fig. 1. Synthetic routes of (a) compound **3**; (b) compound **4**. Compound **3**: c) FT-IR spectrum (CH_2Cl_2 film on KBr pellet). d) ^1H NMR spectrum in DMSO-d_6. Compound **4**: e) FT-IR spectrum (CH_3CN film on NaCl pellet). f) ^1H NMR spectrum in $CDCl_3$.

2.1.7. Cell viability assay

Cell viability was determined using the MTT assay [30]. A total of 10,000 cells were seeded in 96-well plate and treated for 48 h. Organoselenium compounds were dissolved in DMSO at a concentration of 0.01 M. Dose-response curves with 5 concentrations (100, 50, 25, 10 and 1 μM expressed in μg/mL for each compound)) were built for calculate the half maximal inhibitory concentration (IC_{50}). AuNPs-containing Se ligands were dissolved in DMSO at concentration of 10 mg/mL and dose-response curves were obtained with 5 concentrations (100, 50, 25, 10 and 5 μg/mL of Se-loaded and Se-functionalized AuNPs). Dose-response curves of the most active nanoparticles formulation were completed with the concentrations 2.5, 1 and 0.5 μg/mL. After treatment, 20 μL/well of MTT solution in PBS (5 mg/mL) was added and cells were incubated for 2.5 h. Medium was removed and 50 μL/well of DMSO was used to dissolve the formed formazan crystals. The absorbance was measured at 570 nm. The results were expressed as IC_{50}. Values were calculated with the software Origin pro 9.0 by non-linear curve fitting. Three independent experiments were performed.

3. Results and discussion

3.1. Synthesis and characterization of organoselenium compounds

Synthesis of compounds **1** and **2** were done according to previously reported synthetic strategies based on SeO_2 oxidation [29]. Compound **3** (*N*-(4-selenocyanatophenyl)cinnamamide) was synthesized from cinnamoyl chloride (**0**) and 4-selenocyanatoaniline (**1**) in a 1:1 molar ratio (yield = 48 %) (Fig. 1(a)). Compound **4** (*N*-(3-selenocyanatopropyl) cinnamamide) was synthesized from cynnamoyl chloride (**0**) in the presence of 3-bromopropanamine hydrobromide (**0a**), after addition of KSeCN (Fig. 1(b)). The infrared spectrum of compound **3** is reported in Fig. 1(c). Characteristic bands at 1672 cm^{-1} and 2148 cm^{-1} were attributed to the stretching (ν) vibrations of the C═O group of secondary amides, and ν(-C≡N) functional group covalently linked to Se atom, respectively. The two bands at 3285, and 3332 cm^{-1} were assigned to ν(N-H) of amide group. ^{1}H NMR spectrum in deuterated DMSO (Fig. 1 (d)) showed resonances of aromatic ring, and hydrogens linked to C sp^2 at chemical shift in the 6.5–7 ppm range. Resonance of the amide group appears at 10.44 ppm. ^{13}C, ^{77}Se-NMR, and mass spectra are reported in Figure S3. FT-IR spectrum of compound **4** (Fig. 1(e)) showed bands at 3300 cm^{-1} ν(N-H), and 1730 cm^{-1} ν(C═O) due to the presence of a secondary amide. Signals at 2149 cm^{-1} and 3030 cm^{-1} were attributed to ν(-C≡N) and ν(-C-H sp^2), respectively. Differences can be observed in the 2800–2900 cm^{-1} wavenumber region. Compound **4** showed bands at 2933 cm^{-1} due to asymmetric stretching (ν_{as}), and at 2858 cm^{-1} symmetric stretching (ν_s) of -CH_2 of the propyl chain. Signals in the ^{1}H NMR spectrum (Fig. 1(f)) presented typical resonances of the cinnamamide building block. Signals of -CH_2- covalently linked to Se atom and amide group appeared at 2.20 ppm, and 3.57 ppm, respectively. Further characterization of compound **4** (^{13}C, and ^{77}Se-NMR) can be found in Figure S4.

3.2. Synthesis and characterization of Se-functionalized AuNPs

AuNPs functionalized with Se-based ligands, *i.e.*, compounds **1**, **3**, and **4**, were synthesized according to the procedure reported in Fig. 2. AuNPs-**1**, AuNPs-**3**, AuNPs-**4** were obtained with Au/Se 1/4, 1/2, and 1/4 molar ratio, respectively. The UV-Vis spectra showed the LSPR band in the typical range 500–600 nm for AuNPs (spectra are reported in Figure S5, S6 and S7 together with structural and microscopy images). The particle size distribution displayed a dramatically different behavior as structure of Se-based ligands changed. Indeed, recorded hydrodynamic diameter (<$2R_H$>) values were $<2R_H>_{AuNPs\text{-}1} = (80 \pm 30)$ nm (Figure S5), $<2R_H>_{AuNPs\text{-}3} = (525 \pm 185)$ nm (Figure S6), and $<2R_H>_{AuNPs\text{-}4} = (190 \pm 90)$ nm (Figure S7). Bulkiness and electronic nature of surface ligands influence main physicochemical properties of AuNPs, *i.e.*, LSPR band position, particle diameter, and solubility [31]. Compounds **1** and **3** both possess an aromatic ring directly linked to the Se atom, although compound **1** has a primary amine as ending group; thus, with the same molar ratio used in the synthetic procedure the presence of an additional aromatic ring in compound **3** can enhance π–π stacking interactions between ligand molecules on AuNPs surface. As a result, a significant increase in the <$2R_H$> from (80 ± 30) nm to (525 ± 185) nm for AuNPs-**1** and AuNPs-**3**, respectively, occurs. These observations are in agreement with aromatic effect due to the presence of phenyl aromatic ring in Se ligand structure, as reported for analogous phenylthiol, in which electronic conjugation results in bathochromic shift of LSPR and π electrons contribute to favorable ligand-ligand attractions resulting in increased particles size [29]. Compound **4** belongs to alkyl ligands and the aliphatic carbon chain allows higher mobility of ligand tails with weak intermolecular interactions between

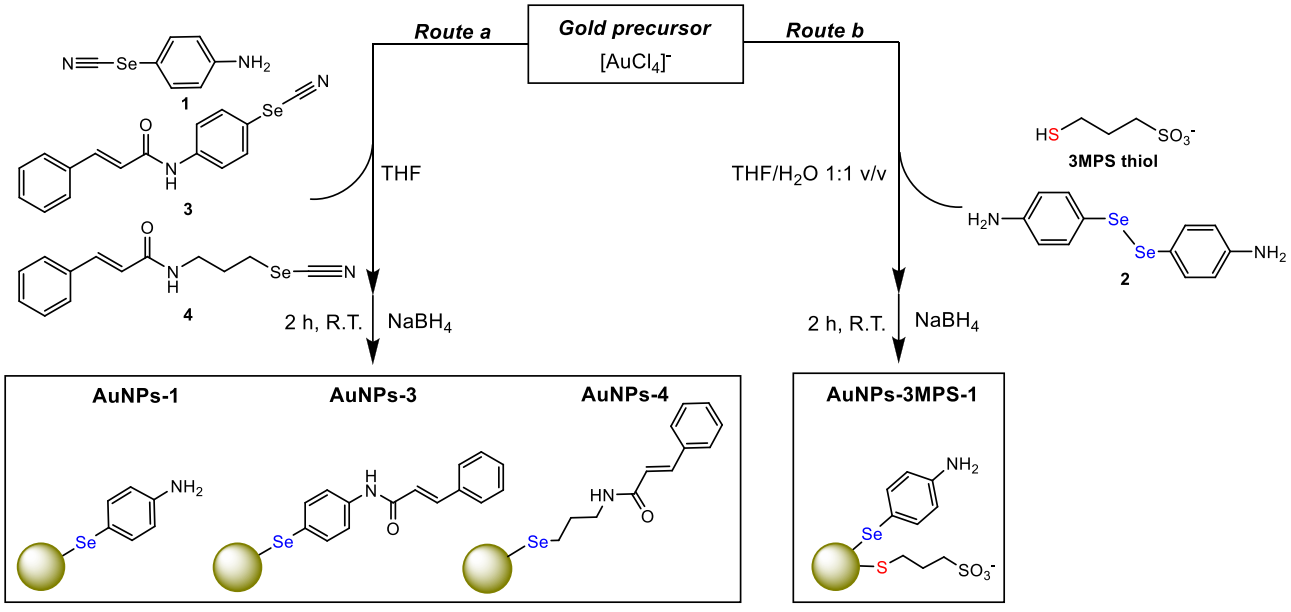

Fig. 2. a) Synthesis procedure of AuNPs-**1**, AuNPs-**3**, AuNPs-**4**, and AuNPs-3MPS-**1**.

functionalizing Seligands. Due to the chemical structures of the Se-based ligands, the as-synthesized AuNPs showed a general suspendability in organic solvents and HCl 1 mM, with little to no solubility in water medium (pH range 6–7.5), crucial parameters for nanomedicine applications.

To enhance the hydrophilic behavior, AuNPs functionalized with mixed ligands, *i.e.*, sodium 3-mercapto-1-propanesulfonate (3MPS) and compound **1**, were synthesized in a water:THF 1:1 v/v mixture. 3MPS, an aliphatic thiol bearing a sulfonate negatively charged end group was chosen to obtain hydrophilic and non-cytotoxic AuNPs [1,32,33]. Compound **2**, a diseleno- derivative, was chosen as precursor of Se ligand, since it decomposes *in-situ via* Se–Se bond cleavages in the presence of excess amount of reducing agents leading to the corresponding compound **1**. A schematic view of the mixed-ligand AuNPs is shown in Fig. 2. The reduction of gold ions into metallic AuNPs-3MPS-**1** gives rise to the formation of a broad UV-Vis absorption band centered at 600 nm and the absorption of both 3MPS thiol and Se ligand on AuNPs surface in the 200–400 nm wavelength region can be observed (Figure S8). DLS results showed a population of AuNPs with $<2R_H>$ = (255 ± 135) nm (Figure S8). Besides, FESEM evidenced the presence of larger aggregates (>100 nm) of isolated AuNPs of diameter in the 5–10 nm range (Figure S8). Tendency towards aggregation at solid state has been confirmed also by AFM (Figure S8), in which a good correlation with FESEM measurements and particles size distribution probed by DLS exist.

Structural characterizations of AuNPs-3MPS-**1** were performed by FT-IR, and synchrotron radiation XPS. The ATR-IR spectrum of AuNPs is presented in Fig. 3(a). The reported spectrum displayed signals at 1032, 1160 cm^{-1} due to the symmetric (ν_s) and asymmetric (ν_{as}) stretching vibrations of sulfonate group (-SO_3^-) of 3MPS, respectively. Signal at 660 cm^{-1} is due to C-S stretching vibration, whereas two bands at 2928 and 2852 cm^{-1} correspond to the ν_{as} and ν_s vibrations of -CH_2- groups of 3MPS aliphatic chain. Intense peaks were also observed at 807 cm^{-1} due to out-of-plane deformation mode of disubstituted aromatic ring, and at 1642 cm^{-1} attributed to the bending vibration of primary aromatic amine of compound **1**. Stretching vibrations of primary amine were found at ν_s = 3304 cm^{-1} and ν_{as} = 3495 cm^{-1}. Weak C-H stretching modes of aromatic ring occurs in the 3000–3100 cm^{-1} wavenumber region. FT-IR spectra of pristine compound **1** and 3MPS thiol are reported in Figure S1 and Figure S9, respectively.

SR-induced XPS measurements were performed at the C1s, N1s, S2p, Se3d and Au4f core levels on AuNPs-3MPS-**1** (BE, FWHM, atomic ratios are reported in Table S1). Se3d spectrum (Fig. 3(b)) consists of two couples of spin-orbit ($Se3d_{5/2}$, $Se3d_{3/2}$) doublets, of which we consider as reference the $Se3d_{5/2}$ component. The $Se3d_{5/2}$ signal at 53.96 eV is relative to Se covalently bonded to AuNP surface [34]. $Se3d_{5/2}$ signal at 55.18 eV is assigned to selenium bonded to carbon atoms [35] S2p spectrum (Fig. 3(c)) is made of five couples of spin-orbit doublets ($S2p_{3/2}$, $S2p_{1/2}$) of which the $S2p_{3/2}$ signal is taken as reference. $S2p_{3/2}$ signal at 161.03 eV is relative to sp hybridized sulfur covalently bonded to gold nanoparticle surface that can be distinguished by S-Au bonds with sp^3 hybridized sulfur at 162.76 eV; $S2p_{3/2}$ signal around 165 eV is assigned to disulfides [36] N1s spectrum (Fig. 3(d)) is associated to the nitrogen atom of Ar-NH_2 of compound **1**.

3.3. Synthesis and characterization of Se-loaded AuNPs

To perform comparative studies in view of biological tests, non-covalent immobilization method was employed to load Se compounds on hydrophilic AuNPs. Gold nanoparticles covalently functionalized with negatively charged 3MPS thiol, *i.e.*, AuNPs-3MPS, were chosen as suitable platform for Se-based compounds immobilization due to their well-assessed hydrophilic and non-cytotoxic nature both *in vitro* and *in vivo* [32,37]. Stock solution of AuNPs-3MPS in ultrapure water (λ_{LSPR} = 520 nm, $<2R_H>$ = (21 ± 7) nm, ζ-potential = (−38 ± 4) mV, Figure S9) were mixed with different solutions of Se compounds, *i.e.*, compound **1**

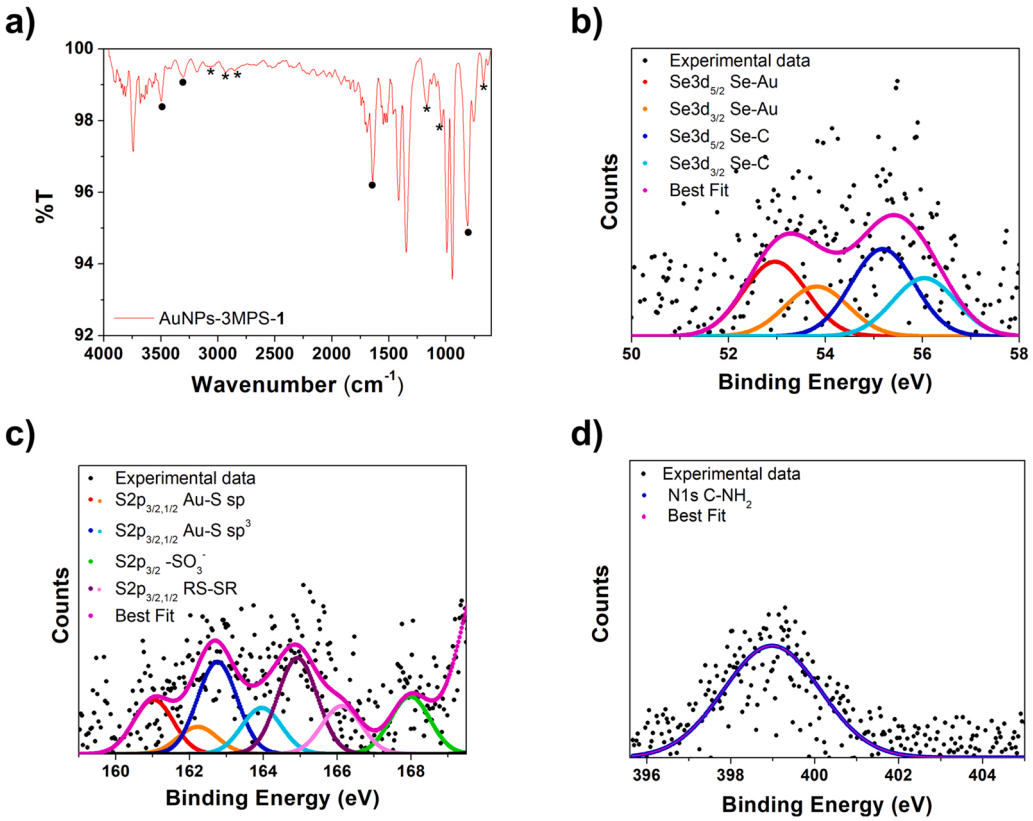

Fig. 3. AuNPs-3MPS-**1** characterizations: a) FTIR spectrum (film from DMSO). XPS spectra: b) Se3d core level, c) S2p core level and d) N1s core level.

in H_2O_{up} at pH 3, compound **3** in DMF, compound **4** in DMF, in a 10:1 weight ratio, as schematically reported in Fig. 4(a). First, the amount of each Se compounds on AuNPs-3MPS surface was assessed by calibration curve and the loading estimated by the equation reported in paragraph 2.1.6: loading of compound **1** = (47 ± 4) %, loading of compound **3** = (64 ± 2) %, and loading of compound **4** = (46 ± 5) % (Fig. 4(b)). The resulting conjugates AuNPs-3MPS@**1**, AuNPs-3MPS@**3**, and AuNPs-3MPS@**4** were further characterized. The UV-Vis spectra of AuNPs-3MPS@**1** (Fig. 4(c)) showed a broad absorption band centered at λ_{max} = 585 nm. The LSPR band of AuNPs-3MPS exhibit a significant red-shift from λ_{LSPR} = 520 nm, *i.e.*, pristine AuNPs-3MPS, up to 585 nm after loading of compound **1**. This behavior can be ascribed to aggregation of smaller NPs into large agglomerates compound **1**-mediated. Indeed, AuNPs-3MPS@**1** give a $<2R_H>$ = (530 ± 205) nm (Fig. 4(f)) and ζ-potential = (−11 ± 3) mV. Loading of compound **3** and compound **4** did not affect the plasmon resonance band of AuNPs-3MPS. Both systems, *i.e.*, AuNPs-3MPS@**3** (Fig. 4(d)), and AuNPs-3MPS@**4** (Fig. 4(e)), showed slightly red-shifted visible band centered at λ_{max} = 525 nm, and at λ_{max} = 535 nm, respectively, whereas loaded compounds **3** and **4** presented intense absorption in the 200–300 nm wavelength range compared to the free ligands. DLS measurements on AuNPs-3MPS@**3**, and AuNPs-3MPS@**4** demonstrated the low hydrodynamic diameters of these systems compared to AuNPs-3MPS@**1**, *i.e.*, $<2R_H>$ = (255 ± 136) nm and $<2R_H>$ = (255 ± 155) nm (Fig. 4(f)), for compound **3**- and compound **4**-loaded AuNPs, respectively. Stability in water was evaluated by ζ-potential measurements and results were as follows: AuNPs-3MPS@**3** ζ-potential = (−29 ± 5) mV, and AuNPs-3MPS@**4** ζ-potential = (−20 ± 6) mV. Increase in the $<2R_H>$ values after immobilization of compounds **3** and **4** is consistent with the non-covalent coating of AuNPs-3MPS core with Se compounds, although a good colloidal stability (ζ-potential over −20 mV) is retained.

SEM images of AuNPs-3MPS@**1** (Figure S11) confirmed the aggregation of small nanoparticles embedded within organic layer. The amorphous organic layer due to immobilization of Se-based compounds

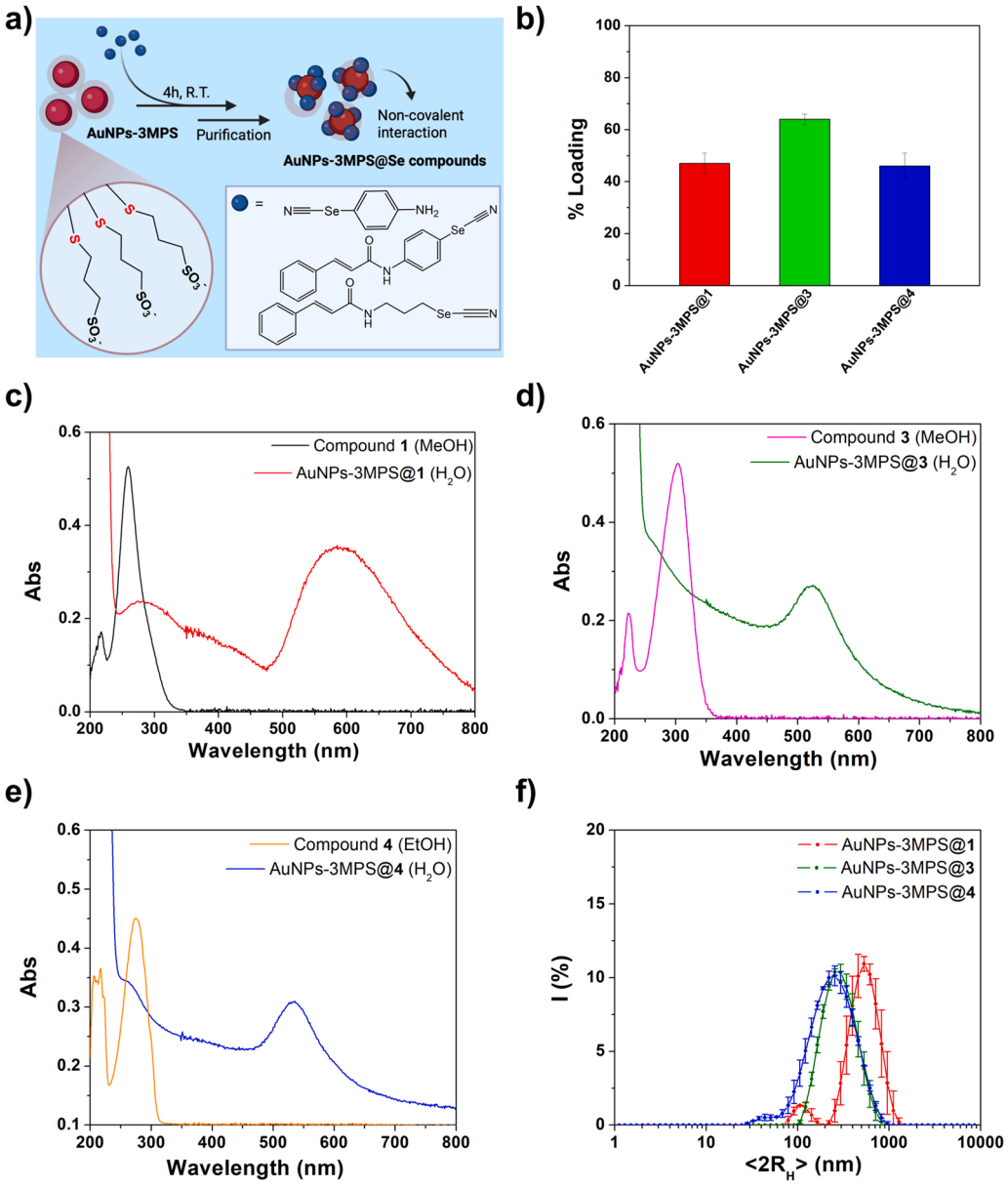

Fig. 4. a) Immobilization scheme of Se compounds on AuNPs-3MPS b) Loading percentage of Se compounds on AuNPs-3MPS. UV-Vis spectra of: c) AuNPs-3MPS@**1** and compound **1**. d) AuNPs-3MPS@**3** and compound **3**. e) AuNPs-3MPS@**4** and compound **4**. f) DLS size distribution of AuNPs-3MPS@**1**, AuNPs-3MPS@**3**, and AuNPs-3MPS@**4**.

can be clearly seen also for AuNPs-3MPS@**3** and AuNPs-3MPS@**4** (Fig. 5 (a,b)). In AFM images of AuNPs-3MPS@**3** and AuNPs-3MPS@**4** (Fig. 5(c, d)) the above mentioned amorphous organic layer appears as a carpet-like structure ubiquitously diffused on all the surface of the glass substrate, particularly in the case of AuNPs-3MPS@**3**. Both techniques showed spherical-shaped AuNPs with diameter below 10 nm, coherently with the dimensions of the pristine AuNPs-3MPS (Figure S10).

Advanced structural characterizations were performed on all the systems, *i.e.*, AuNPs-3MPS@**1**, AuNPs-3MPS@**3**, and AuNPs-3MPS@**4**, by SR-XPS at the C1s, N1s, O1s, S2p, Se3d and Au4f core levels. Prior to immobilization, AuNPs-3MPS were characterized at S2p and Au4f core level considered as the most indicative for the assessment of AuNPs functionalization (Table S2). S2p spectrum of AuNPs-3MPS reported in Figure S12 consisted of four spin-orbit pairs, individuated applying a peak-fitting procedure. Starting from the peaks at lower BE values, the four S2p components can be attributed to: RS-Au (3MPS thiol molecules covalently linked to gold atoms at the NPs surface) ($S2p_{3/2}$ BE = 161.40 eV), physisorbed RSH thiol groups ($S2p_{3/2}$ BE = 163.02 eV), and sulfonate functional groups of 3MPS at 166.86 eV and at 168.46 eV for -SO_3- and -SO_3Na, respectively, as already observed for analogous systems [1]. SR-XPS characterization of AuNPs-3MPS@**1**, and AuNPs-3MPS@**4** are reported in Figure S13-S14, respectively. SR-XPS data (BE, FWHM, atomic ratios) of AuNPs-3MPS@**3** are reported in Table S3. Se3d spectrum (Fig. 6(a)) was made of two couples of spin-orbit ($Se3d_{5/2}$, $Se3d_{3/2}$) doublets, of which we consider as reference the $Se3d_{5/2}$ component. $Se3d_{5/2}$ signal at 55.45 eV was assigned to selenium bonded to carbon atoms of Se ligand confirming the non-covalent interaction of compound **3** with thiol-capped AuNPs surface [33]. Signals due to Se-Se intermolecular interaction of Se compounds were found in both AuNPs-3MPS@**1** (Figure S13) and AuNPs-3MPS@**4** (Figure S14) together with Se-C peaks centered at 55.69 eV, and 55.22 eV, respectively [38]. N1s spectrum (Fig. 6) was made of two components at 399.39 eV is associated to nitrogen atom of -C≡N group, and at 401.46 eV assigned to the nitrogen atom of secondary amide (-NH(CO)) [39]. N1s data of AuNPs-3MPS@**1**, and AuNPs-3MPS@**2** can be found in Table S4-S5.

S2p spectrum of AuNPs-3MPS@**3** was made of five couples of spin-orbit doublets ($S2p_{3/2}$, $S2p_{1/2}$) of which the $S2p_{3/2}$ signal was taken as reference (Table S3). $S2p_{3/2}$ signal at 161.73 eV was associated to sulfur of 3MPS thiol covalently linked to the gold surface of nanoparticles. $S2p_{3/2}$ signal at 163.23 eV was assigned to physisorbed thiols and $S2p_{3/2}$ signal at 164.17 eV was assigned to thiol end group giving rise to disulfides [40].

Au4f spectrum of AuNPs-3MPS@**3** (Figure S15) and AuNPs-3MPS@**1** (Figure S13) showed two couples of spin-orbits ($Au4f_{7/2}$, $Au4f_{5/2}$) doublets, of which we consider as reference the $Au4f_{7/2}$ component. The $Au4f_{7/2}$ signal at 84.00 eV was due to metallic bulk Au(0) atoms of NPs, whereas the peak at 84.8 eV was assigned to surface Au atoms of AuNPs involved in the S-Au bonds.

3.4. Stability of AuNPs-3MPS conjugates in water

To determine the stability of AuNPs-3MPS@**1**, and AuNPs-3MPS@**4**, nanoparticles were suspended in H_2O_{up} at pH 7 (1 mg/mL) and release of Se compounds non-covalently linked to AuNPs surface measured spectrophotometrically. The cumulative percentage of Se-compounds released from AuNPs at 37 °C and different time intervals is shown in Figure S16. As reported, the release did not reach 100 % under these circumstances. Due to non-covalent interaction between AuNPs-3MPS and organoselenium compounds, the release of loaded molecules is a diffusion-controlled process; thus, at physiological pH value AuNPs-3MPS@**4** maintain their stability within 24 h. By contrast, for AuNPs-3MPS@**1** 60 % of the loaded compound **1** was released within the first 24 h. Differences in the stability of the two AuNPs-3MPS@**1**, and AuNPs-3MPS@**4** conjugates can be ascribed to synergistic effect of (i) size of the ligand, and (ii) intermolecular Se···Se interactions surface between ligand molecules close to the AuNPs-3MPS surface. According to SR-XPS results (see paragraph 3.3), compound **4** experienced pronounced interaction between nearby Se atoms compared to compound **1**. As for diffusion-controlled processes, the release rate is affected by steric hindrance and size of the ligands. Indeed, bulky compound **4** showed a slow release (<10 % in 24 h), whereas the smaller compound **1** was quickly released within 24 h.

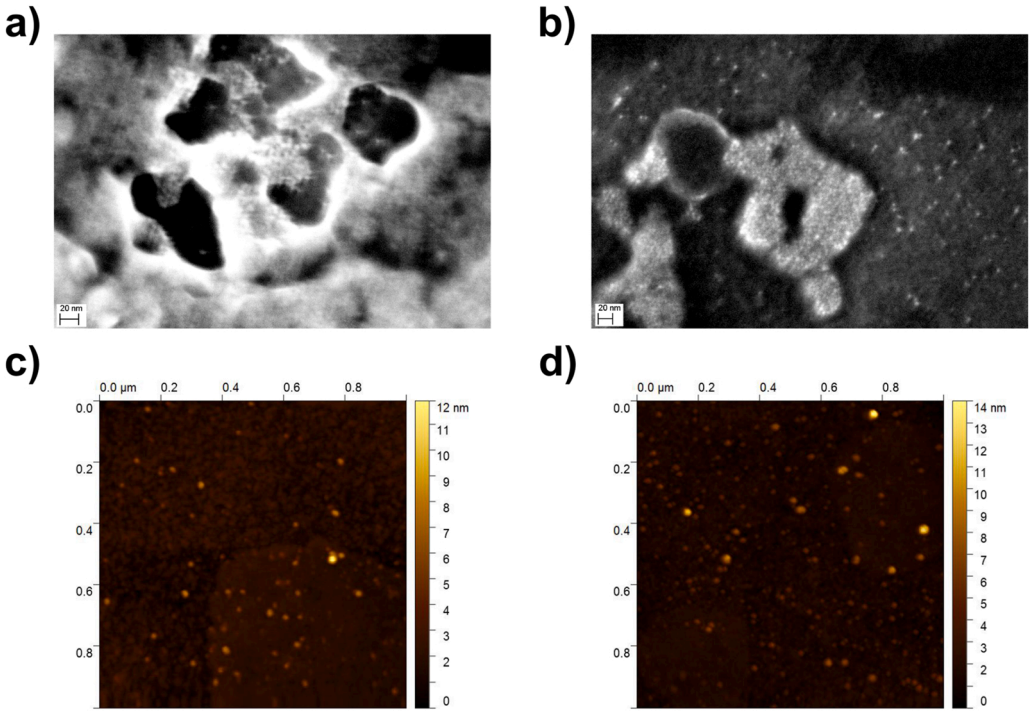

Fig. 5. a) FESEM image of AuNPs-3MPS@**3**. b) FESEM image of AuNPs-3MPS@**4**. c) AFM image of AuNPs-3MPS@**3**. d) AFM image of AuNPs-3MPS@**4**.

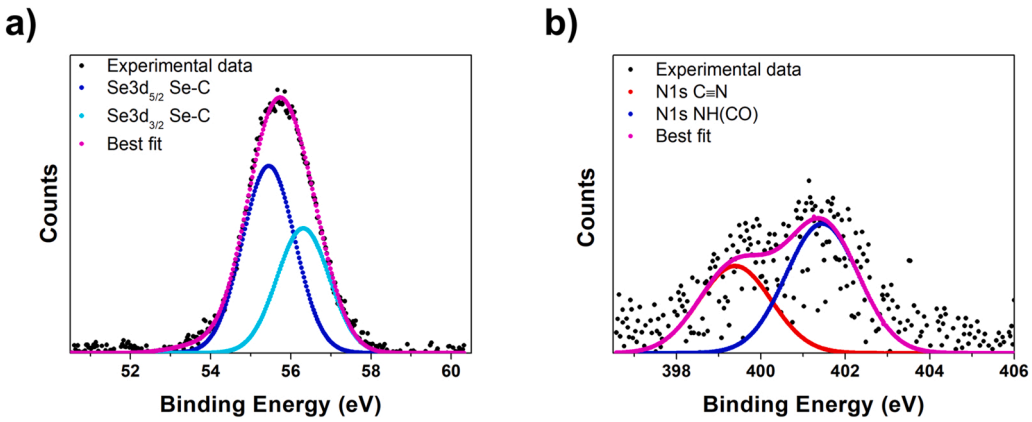

Fig. 6. XPS spectrum of AuNPs-3MPS@**3** at a) Se3d and b) N1s core level.

3.5. *In vitro biological studies of Se-loaded and Se-functionalized AuNPs*

Pristine compounds **1**, **2**, **3**, and **4**, and their conjugates with AuNPs-3MPS were tested against two different tumor cell lines: PC-3 (prostatic adenocarcinoma), and HCT-116 (colorectal carcinoma). *In vitro* biological evaluations were performed at 48-h treatment with MTT assay. IC_{50} values were calculated from dose-response curves in the 0–100 μg/mL concentration range and values are reported in Table 1. Based on literature, compound **1** (a selenocyanate) and **2** (a diselenide), showed anticancer activity [29]. Both compounds presented moderate activity in HCT-116 cell line. On PC-3 cell line, compound **1** showed comparable biological activity, although compound **2** revealed an enhancement of its cytotoxicity compared to treatment on HCT-116 cells (Figure S17). *In vitro* experiments on free compounds **3** and **4** were also performed. In PC-3 cells, both compounds **3** and **4**, showed comparable cytotoxicity with IC_{50} values of (10.2 ± 0.7) μg/mL and (11 ± 4) μg/mL, respectively. In the HCT-116 cell lines, compound **4** showed higher cytotoxicity. Besides, for free compound **3** no cytotoxicity effect was reported on HCT-116. Dose-response curves of compounds **3** and **4** are reported in Figure S17. For comparison, Se-loaded and Se-functionalized AuNPs were tested in *vitro* on PC-3, and HCT-116 cell lines. AuNPs-**1**, and AuNPs-**3**, in which Se-Au covalent bonds exist, showed an IC_{50} value above the concentration range explored (>100 μg/mL); thus, no cytotoxic effect was reported in both cell lines. AuNPs-3MPS-**1** sample displayed an IC_{50} = (62 ± 10) μg/mL selectively in the HCT-116 cell line, whereas no cytotoxic activity was reported in PC-3 cells. Immobilization of Se compounds on previously synthesized AuNPs-3MPS, *i.e.*, AuNPs-3MPS@**1**, AuNPs-3MPS@**3**, and AuNPs-3MPS@**4**, led to different biological activity compared to pristine compounds. Similar biological activity was observed after treatment with AuNPs-3MPS@**1** (IC_{50} = 6.0 ± 0.5 μg/mL in PC-3, IC_{50} = 5.5 ± 0.3 μg/mL in HCT-116) and AuNPs-3MPS@**3** (IC_{50} = 4.2 ± 0.5 μg/mL in PC-3, IC_{50} = 3.6 ± 0.2 μg/mL in HCT-116) in both cell lines. AuNPs-3MPS@**4** sample showed higher cytotoxicity in HCT-116 cells (IC_{50} = 4.9 ± 0.8 μg/mL) compared to PC-3 cell line (IC_{50} = 8 ± 1 μg/mL). It is noteworthy that immobilization procedure notably enhances the cytotoxic effect of compounds **1**, **3** and **4** on both cell lines compared to free compounds. Although the IC_{50} values (expressed as μg/mL) are similar, the amount of each compound inside the AuNPs-3MPS is much lower than the concentration of free compounds needed to induce a 50 % cell growth inhibition (Table S6). The potent cytotoxic activity observed after the immobilization procedure is determined by neither the presence of the selenocompounds nor the AuNPs-3MPS, but from the whole system. Compound **3** showed noticeable cytotoxicity on HCT-116 cell line only after the immobilization, whereas no toxicity was reported for the pristine compound **3**. Anticancer activity in Se-based organic compounds is mainly associated with ROS generation by Se atom [41]. Due to that, functionalization of AuNPs with Se ligands, with the formation of a covalent bond between Se ligands and gold nanoparticles, *i.e.*, AuNPs-**1**, AuNPs-**3**, AuNPs-3MPS-**1**, gave little to no anticancer activity in the concentration range explored. Besides, immobilization of Se compounds on ready-to-use hydrophilic AuNPs-3MPS allowed to maintain the Se exposition to cellular environment, exploiting their biological activity. High surface-*to*-volume ratio of AuNPs increases the local concentration of bioactive molecules, thus enhancing the antitumoral effect compared to free compounds. These *in vitro* results showed that gold nanoparticles could significantly improve the cytotoxic effect of Se compounds at lower concentration compared to free compounds. In view of *in vivo* biomedical applications, enhancing the cytotoxic effect of active molecules will allow to reduce the administered dose, reducing dose-related toxicity.

Table 1
IC_{50} (μg/mL) values obtained from MTT assay on PC-3 and HCT-116 cell lines.

	IC_{50} (μg/mL)	
	PC-3 cell line	HCT-116 cell line
Compound **1**	3.9 ± 0.7	3.1 ± 0.6
Compound **2**	3.1 ± 0.4	7.5 ± 0.1
Compound **3**	10.2 ± 0.7	>100
Compound **4**	9.7 ± 0.1	3.2 ± 0.9
AuNPs-**1**	>100	>100
AuNPs-**3**	>100	>100
AuNPs-3MPS-**1**	>100	62 ± 10
AuNPs-3MPS@**1**	6.0 ± 0.5	5.5 ± 0.3
AuNPs-3MPS@**3**	4.2 ± 0.5	3.6 ± 0.2
AuNPs-3MPS@**4**	8 ± 1	4.9 ± 0.8

3.6. *Conclusions*

AuNPs functionalized with organoselenium compounds were obtained through two different approaches. AuNPs properties and morphology were evaluated. Results demonstrated that the direct conjugation method led to the formation of aggregated AuNPs with poor solubility in water. To improve their stability, mixed AuNPs-3MPS-**1** were synthesized. Immobilization procedure to obtain AuNPs-3MPS@**1**, AuNPs-3MPS@**2**, and AuNPs-3MPS@**4** conjugates allowed a non-covalent coating of non-cytotoxic AuNPs-3MPS with Se compound. Stability studies in water in the 0–24-h time scale demonstrated that AuNPs-3MPS@**4** was the most stable conjugate with release <10 %. All the systems were screened against PC-3 and HCT-116 cell lines. Selective anticancer effect on HCT-116 cell line was obtained in case of AuNPs-3MPS-**1**. Despite similar IC_{50} values, the AuNPs-3MPS@Se compounds allowed to obtain 50 % of cell growth inhibition with lower amount of Se compounds compared to unloaded compounds or free AuNPs-3MPS. Different cytotoxic effect can be ascribed to the exposure of Se atoms as supported by SR-XPS studies. Results of this study demonstrated that

AuNPs represent a suitable platform to influence the *in vitro* response of the organoselenium compounds.

Declaration of Competing Interest

The authors declare that they have no known competing financial interests or personal relationships that could have appeared to influence the work reported in this paper.

Data availability

Data will be made available on request.

Acknowledgements

Authors acknowledge Dr. Paolo Lacovig at SuperESCA beamline (SR-XPS measurements), Ateneo Sapienza 2019 (RM11916B75D8FAF5), Ateneo Sapienza 2020 (RM120172B6B660AB) for funding and the CERIC-ERIC Consortium for the access to the experimental facility SuperESCA@Elettra and financial support (CERIC proposal #20202004).

CRediT authorship contribution statement

Sara Lorenzoni: Investigation, Visualization. **Sara Cerra**: Investigation, Writing - Original Draft. **Eduardo Angulo-Elizari**: Investigation, Visualization. **Tommaso A. Salamone**: Investigation, Visualization. **Chiara Battocchio**: Investigation, Visualization. **Martina Marsotto**: Investigation, Visualization. **Francesca A. Scaramuzzo**: Investigation, Visualization. **Carmen Sanmartín**: Visualization. **Daniel Plano**: Conceptualization, Supervision, Writing - Review & Editing. **Ilaria Fratoddi**: Conceptualization, Supervision, Writing - Review & Editing.

References

[1] S. Cerra, R. Matassa, A.M. Beltrán, G. Familiari, C. Battocchio, I. Pis, F. Sciubba, F. A. Scaramuzzo, A. Del Giudice, I. Fratoddi, Insights about the interaction of methotrexate loaded hydrophilic gold nanoparticles: Spectroscopic, morphological and structural characterizations, Mater. Sci. Eng. C 117 (2020), 111337, https://doi.org/10.1016/j.msec.2020.111337.

[2] F.Y. Kong, J.W. Zhang, R.F. Li, Z.X. Wang, W.J. Wang, W. Wang, Unique roles of gold nanoparticles in drug delivery, targeting and imaging applications, Molecules 22 (2017) 9, https://doi.org/10.3390/molecules22091445.

[3] X. Ou, Y. Liu, M. Zhang, L. Hua, S. Zhan, Plasmonic gold nanostructures for biosensing and bioimaging, Microchim. Acta 188 (2021) 304, https://doi.org/10.1007/s00604-021-04964-1.

[4] C. Lu, S. Zhou, F. Gao, J. Lin, J. Liu, J. Zheng, DNA-mediated growth of noble metal nanomaterials for biosensing applications, Trends Anal. Chem. 148 (2022), 116533, https://doi.org/10.1016/j.trac.2022.116533.

[5] A. Narmani, M. Rezvani, B. Farhood, P. Darkhor, J. Mohammadnejad, B. Amini, S. Refahi, N. Abdi Goushbolagh, Folic acid functionalized nanoparticles as pharmaceutical carriers in drug delivery systems, Drug Dev. Res. 80 (2019) 404–424, https://doi.org/10.1002/ddr.21545.

[6] N. Nashat, Z. Haider, A Review on gold nanoparticles (GNPs) and their advancement in cancer therapy, Int. J. Nanomater. Nanotechnol. Nanomed. 7 (2021) 19–25, https://doi.org/10.17352/2455-3492.000040.

[7] D. Kalyane, N. Raval, R. Maheshwari, V. Tambe, K. Kalia, R.K. Tekade, Employment of enhanced permeability and retention effect (EPR): Nanoparticle-based precision tools for targeting of therapeutic and diagnostic agent in cancer, Mater. Sci. Eng. C 98 (2019) 1252–1276, https://doi.org/10.1016/j.msec.2019.01.066.

[8] R.L.C.G. da Silva, K. de Oliveira Gonçalves, L.C. Courrol, L. Caseli, Study of the interactions of gold nanoparticles functionalized with aminolevulinic acid in membrane models, Colloids Surf. B 205 (2021), 111849, https://doi.org/10.1016/j.colsurfb.2021.111849.

[9] D.F. Baez, E. Gallardo-Toledo, M.P. Oyarzun, E. Araya, M.J. Kogan, The influence of size and chemical composition of silver and gold nanoparticles on in vivo toxicity with potential applications to central nervous system diseases, Int. J. Nanomed. 16 (2021) 2187–2201, https://doi.org/10.2147/IJN.S260375.

[10] D. Peixoto, I. Pereira, M. Pereira-Silva, F. Veiga, M.R. Hamblin, Y. Lvov, M. Liu, A. C. Paiva-Santos, Emerging role of nanoclays in cancer research, diagnosis, and therapy, Coord. Chem. Rev. 440 (2021), 213956, https://doi.org/10.1016/j.ccr.2021.213956.

[11] P.S. Sadalage, R.V. Patil, D.V. Havaldar, S.S. Gavade, A.C. Santos, K.D. Pawar, Optimally biosynthesized, PEGylated gold nanoparticles functionalized with quercetin and camptothecin enhance potential anti-inflammatory, anti-cancer and anti-angiogenic activities, J. Nanobiotechnology 19 (2021) 84, https://doi.org/10.1186/s12951-021-00836-1.

[12] J. Nellore, P.C. Pauline, K. Amarnath, Biogenic synthesis by sphearanthus amaranthoids; towards the efficient production of the biocompatible gold nanoparticles, Dig. J. Nanomater. Biostructures 4 (2009) 557–563, https://doi.org/10.1007/s40097-018-0267-4.

[13] A.C. Paiva Santos, A.M. Herdade, C. Guerra, D. Peixoto, M. Pereira-Silva, M. Zeinali, F. Mascarenhas-Melo, A. Paranhos, F. Veiga, Int. J. Pharm. 597 (2021), 120311.

[14] D. Ungor, I. Dékány, E. Csapó, Reduction of tetrachloroaurate(III) ions with bioligands: role of the thiol and amine functional groups on the structure and optical features of gold nanohybrid systems, Nanomaterials 9 (2019) 1229, https://doi.org/10.3390/nano9091229.

[15] E. Pensa, E. Corte, M.H. Fonticelli, G. Benítez, A. Rubert, R.C. Salvarezza, The chemistry of the sulfur-gold interface: in search of a unified model, Acc. Chem. Res. 45 (2012) 1183–1192, https://doi.org/10.1021/ar200260p.

[16] K. Priyadarsini, B.G. Singh, P.P. Phadnis, K.C. Barick, P.A. Hassan, Nanoparticle conjugates of selenium compounds: preparation, characterisation and electron transfer reactions, Chem. Proc. 2 (2020) 24, https://doi.org/10.3390/ECCS2020-07545.

[17] T. Li, F. Li, W. Xiang, Y. Yi, Y. Chen, L. Cheng, Z. Liu, H. Xu, Selenium-containing amphiphiles reduced and stabilized gold nanoparticles: kill cancer cells via reactive oxygen species, ACS Appl. Mater. Interfaces 8 (2016) 22106–22112, https://doi.org/10.1021/acsami.6b08282.

[18] P.A. Tsuji, D. Santesmasses, B.J. Lee, V.N. Gladyshev, D.L. Hatfield, Historical roles of selenium and selenoproteins in health and development: the good, the bad and the ugly, Int. J. Mol. Sci. 23 (2022) 5, https://doi.org/10.3390/ijms23010005.

[19] H. Chuai, S.-Q. Zhang, H. Bai, J. Li, Y. Wang, J.S.E. Wen, J. Zhang, M. Xin, Small molecule selenium-containing compounds: recent development and therapeutic applications, Eur. J. Med. Chem. 223 (2021), 113621, https://doi.org/10.1016/j.ejmech.2021.113621.

[20] D. Radomska, R. Czarnomysy, D. Radomski, K. Bielawski, Selenium compounds as novel potential anticancer agents, Int. J. Mol. Sci. 22 (2021) 1–27, https://doi.org/10.3390/ijms22031009.

[21] S.J. Kim, M.C. Choi, J.M. Park, A.S. Chung, Antitumor effects of selenium, Int. J. Mol. Sci. 22 (2021) 0, https://doi.org/10.3390/ijms22210000.

[22] V. Gandin, P. Khalkar, J. Braude, A.P. Fernandes, Organic selenium compounds as potential chemotherapeutic agents for T improved cancer treatment, Free Rad. Biol. Med. 127 (2018) 80–97, https://doi.org/10.1016/j.freeradbiomed.2018.05.001.

[23] L. Kuršvietiene, A. Mongirdiene, J. Bernatoniene, J. Šulinskiene, I. Staneviciene, Selenium anticancer properties and impact on cellular redox status, Antioxidants 9 (2020) 80, https://doi.org/10.3390/antiox9010080.

[24] M.D. Kostić, V.M. Divac, Diselenides and selenocyanates as versatile precursors for the synthesis of pharma- ceutically relevant compounds, Curr. Org. Synth. 17 (2020) 0, https://doi.org/10.2174/1570179418666210303113723.

[25] Y. Nie, M. Zhong, S. Li, X. Li, Y. Zhang, Y. Zhang, X. He, Synthesis and potential anticancer activity of some novel selenocyanates and diselenides, Chem. Biodivers. 17 (2020), e1900603, https://doi.org/10.1002/cbdv.201900603.

[26] L. Kong, Q. Yuan, H. Zhu, Y. Li, Q. Guo, Q. Wang, X. Bi, X. Gao, The suppression of prostate LNCaP cancer cells growth by Selenium nanoparticles through Akt/Mdm2/AR controlled apoptosis, Biomaterials 32 (2011) 6515–6522, https://doi.org/10.1016/j.biomaterials.2011.05.032.

[27] S. Shaaban, A.M. Ashmawy, A. Negm, L.A. Wessjohann, Synthesis and biochemical studies of novel organic selenides with increased selectivity for hepatocellular carcinoma and breast adenocarcinoma, Eur. J. Med. Chem. 179 (2019) 515–526, https://doi.org/10.1016/j.ejmech.2019.06.075.

[28] M. Díaz, R. González, D. Plano, J.A. Palop, C. Sanmartín, I. Encío, A diphenyldiselenide derivative induces autophagy via JNK in HTB-54 lung cancer cells, J. Cell. Mol. Med. 22 (2018) 289–301, https://doi.org/10.1111/jcmm.13318.

[29] D. Plano, Y. Baquedano, D. Moreno-Mateos, M. Font, A. Jiménez-Ruiz, J.A. Palop, C. Sanmartín, Selenocyanates and diselenides: a new class of potent antileishmanial agents, Eur. J. Med. Chem. 46 (2011) 3315–3323, https://doi.org/10.1016/j.ejmech.2011.04.054.

[30] T. Mosmann, Rapid colorimetric assay for cellular growth and survival: application to proliferation and cytotoxicity assays, J. lmmunol. Methods 65 (1983) 55–63, https://doi.org/10.1016/0022-1759(83)90303-4.

[31] M. Rambukwella, N.A. Sakthivel, J.H. Delcamp, L. Sementa, A. Fortunelli, A. Dass, Ligand structure determines nanoparticles' atomic structure, metal-ligand interface and properties, Front. Chem. 6 (2018) 330, https://doi.org/10.3389/fchem.2018.00330.

[32] H. Bessar, I. Venditti, L. Benassi, C. Vaschieri, P. Azzoni, G. Pellacani, C. Magnoni, E. Botti, V. Casagrande, M. Federici, A. Costanzo, L. Fontana, G. Testa, F. F. Mostafa, S.A. Ibrahim, M.V. Russo, I. Fratoddi, Functionalized gold nanoparticles for topical delivery of methotrexate for the possible treatment of psoriasis, Colloids Surf. B 141 (2016) 141–147, https://doi.org/10.1016/j.colsurfb.2016.01.021.

[33] I. Venditti, A. Cartoni, S. Cerra, R. Fioravanti, T.A. Salamone, F. Sciubba, M. A. Tabocchini, V. Dini, C. Battocchio, G. Iucci, L. Carlini, R. Faccini, F. Collamati, C. Mancini Terracciano, E. Solfaroli Camillocci, S. Morganti, A. Giordano, T. Scotognella, D. Maccora, D. Rotili, C. Marchese, E. Anastasiadou, P. Trivedi, I. Fratoddi, Hydrophilic gold nanoparticles as anti-PD-L1 antibody carriers: synthesis and interface properties, Part. Part. Syst. Charact. 39 (2022) 2100282, https://doi.org/10.1002/ppsc.202100282.

[34] E. de la Llave, D.A. Scherlis, Selenium-based self-assembled monolayers: the nature of adsorbate-surface interactions, Langmuir 26 (2010) 173–178, https://doi.org/10.1021/la903660y.
[35] F. Li, T. Li, C. Sun, J. Xia, Y. Jiao, H. Xu, Selenium-doped carbon quantum dots (Se-CQDs) for free radical scavenging, Angew. Chem. 129 (2017) 33, https://doi.org/10.1002/anie.201705989.
[36] P. Prosposito, L. Burratti, A. Bellingeri, G. Protano, C. Faleri, I. Corsi, C. Battocchio, G. Iucci, L. Tortora, V. Secchi, S. Franchi, I. Venditti, Bifunctionalized silver nanoparticles as Hg^{2+} plasmonic sensor in water: synthesis, characterizations, and ecosafety, Nanomaterials 9 (2019) 1353, https://doi.org/10.3390/nano9101353.
[37] I. Fratoddi, L. Benassi, E. Botti, C. Vaschieri, I. Venditti, H. Bessar, M.A. Samir, P. Azzoni, C. Magnoni, A. Costanzo, V. Casagrande, M. Federici, L. Bianchi, G. Pellacani, Effects of topical methotrexate loaded gold nanoparticle in cutaneous inflammatory mouse model, Nanomedicine 17 (2019) 276–286, https://doi.org/10.1016/j.nano.2019.01.006.
[38] J. Jia, A. Bendounan, H.M.N. Kotresh, K. Chaouchi, F. Sirotti, S. Sampath, V. A. Esaulov, Selenium adsorption on Au(111) and Ag(111) surfaces: adsorbed selenium and selenide films, J. Phys. Chem. C 117 (2013) 9835–9842, https://doi.org/10.1021/jp4007203.
[39] R.J.J. Jansen, H.Van Bekum, Xps of nitrogen-containing functional groups on activated carbon, Carbon 33 (1995) 1021–1027.
[40] C. Battocchio, F. Porcaro, S. Mukherjee, E. Magnano, S. Nappini, I. Fratoddi, M. Quintiliani, M.V. Russo, G. Polzonetti, Gold nanoparticles stabilized with aromatic thiols: interaction at the molecule-metal interface and ligand arrangement in the molecular shell investigated by SR-XPS and NEXAFS, J. Phys. Chem. C 118 (2014) 8159–8168, https://doi.org/10.1021/jp4126057.
[41] L. Kuršvietienė, A. Mongirdienė, J. Bernatonienė, J. Šulinskienė, I. Stanevičienė, Selenium anticancer properties and impact on cellular redox status, Antioxidants 9 (2020) 80, https://doi.org/10.3390/antiox9010080.